EDGE ARTICLE

Check for updates

The fine effects of high magnetic fields on hyperfine shifts

Letizia Fiorucci, [ID] *[abc] Lucas Lang, [ID] *[d] David L. Tierney,[e] Mauro Botta, [ID] [f] Giacomo Parigi, [ID] [ab] Claudio Luchinat [ID] [abg] and Enrico Ravera [ID] *[abh]

We report a comprehensive investigation of the magnetic field dependence of NMR hyperfine shifts in paramagnetic systems, a critical observable in the study of molecular magnetism. By combining high-field NMR experiments with quantum chemical calculations, we demonstrate that hyperfine shifts exhibit a measurable dependence on the external field. This dependence arises from the interplay between partial molecular alignment and the nonlinear response of the induced magnetic field to the applied magnetic field. We consistently observe a systematic decrease in shifts at higher fields, indicating that the nonlinear contribution is the dominant mechanism. This effect is particularly strong in lanthanoid complexes, where the relative reduction of the shift is primarily determined by the central metal ion. For transition metals, the field dependence depends on the balance of contact and pseudocontact shifts, providing new constraints to check computational protocols.

1 Introduction

NMR is arguably the most informative spectroscopic technique available to chemists, as it affords reliably and reproducibly qualitative and quantitative information on the samples under investigation. Qualitative, because every molecule has its spectral fingerprint, which differs from that of any other molecule. Quantitative, because there is not a specific molar extinction coefficient different from one molecule to another, but the response of a component depends on the number of spins in a particular environment (although this might not be actually feasible under any condition for any spin type). Despite the broad applicability and power, all NMR-based techniques are limited by the intrinsically low sensitivity. This is due to the limited difference in energy–and thus in Boltzmann population–between Zeeman-split nuclear spin states. This problem can be mitigated,

at least in part, by increasing the energy difference by increasing the static magnetic field (B_0). With this, not only the sensitivity increases, but also the spectral resolution is improved, especially for quadrupolar nuclei that vastly benefit from an increase in the magnetic field.[1] As a consequence, higher and higher magnetic field setups have been designed and constructed. The development of new superconducting ceramic oxides that maintain superconductivity in fields up to 40 T has allowed for the development of a new generation of NMR instrumentation.[2,3] It is important to recall that shared research facilities provide broad, affordable access to high-field instruments that are often impractical for individual laboratories to purchase, operate, or sustain independently. The technology is also complemented by dedicated technical expertise, which minimizes the burden of the calibration that is required to reliably observe minute effects.[3–5] The increase in the attainable fields, in turn, has promoted the re-examination of the dependence of the NMR observables on the magnetic field. For chemical shifts, this was originally predicted by Ramsey in 1970 for diamagnetic molecules,[6] and observed by Bendall and Doddrell.[7] The topic has been debated at length,[8–13] until recently, when a brilliant investigation by Vaara, Jokisaari and co-workers reconciled the theory and experiments.[14]

The paramagnetic side of the story was much less investigated. The field dependence in the case of paramagnetic compounds is clearly visible when superimposing spectra of the same metal complex acquired at different magnetic fields: the peaks become narrower because transverse relaxation for small molecules has a dominant field-independent component (see chapter 4 in ref. 15), and the chemical shifts appear smaller in absolute value (as illustrated in Fig. 1).

[a]Department of Chemistry "Ugo Schiff" and Magnetic Resonance Center (CERM), University of Florence, Florence 50019, Italy

[b]Consorzio Interuniversitario Risonanze Magnetiche di Metalloproteine (CIRMMP), Florence 50019, Italy

[c]Max-Planck-Institut für Kohlenforschung, Kaiser-Wilhelm-Platz 1, Mülheim an der Ruhr 45470, Germany. E-mail: fiorucci@kofo.mpg.de

[d]Technische Universität Berlin, Institut für Chemie, Theoretische Chemie/Quantenchemie, Sekr. C7, Straße des 17. Juni 135, Berlin 10623, Germany. E-mail: lucas.lang@chem.tu-berlin.de

[e]Department of Chemistry and Biochemistry, Miami University, Oxford, OH 45056, USA

[f]Dipartimento di Scienze e Innovazione Tecnologica, Università del Piemonte Orientale, Alessandria, Italy

[g]Giotto Biotech S.R.L., Sesto Fiorentino, 50019, Italy

[h]Florence Data Science, University of Florence, Florence 50134, Italy. E-mail: enrico.ravera@unifi.it; ravera@cerm.unifi.it
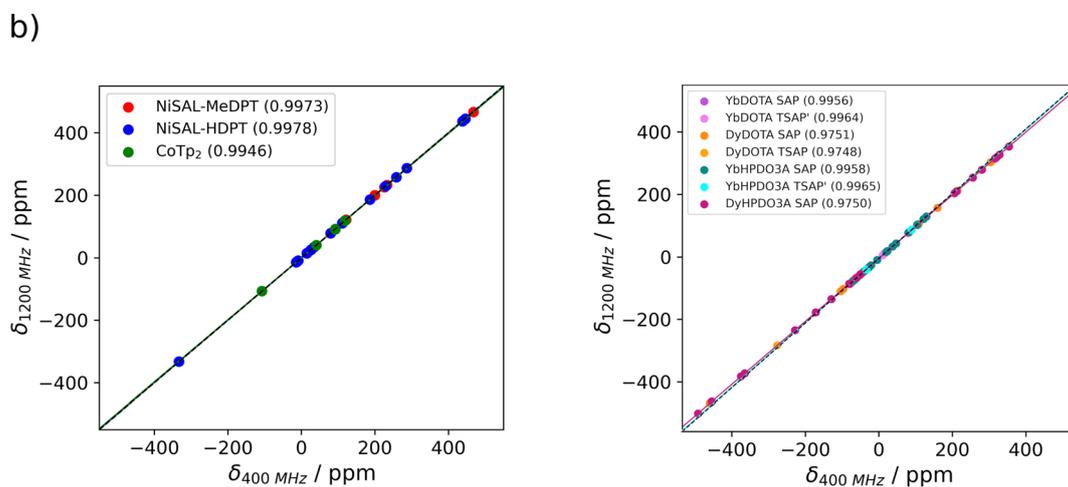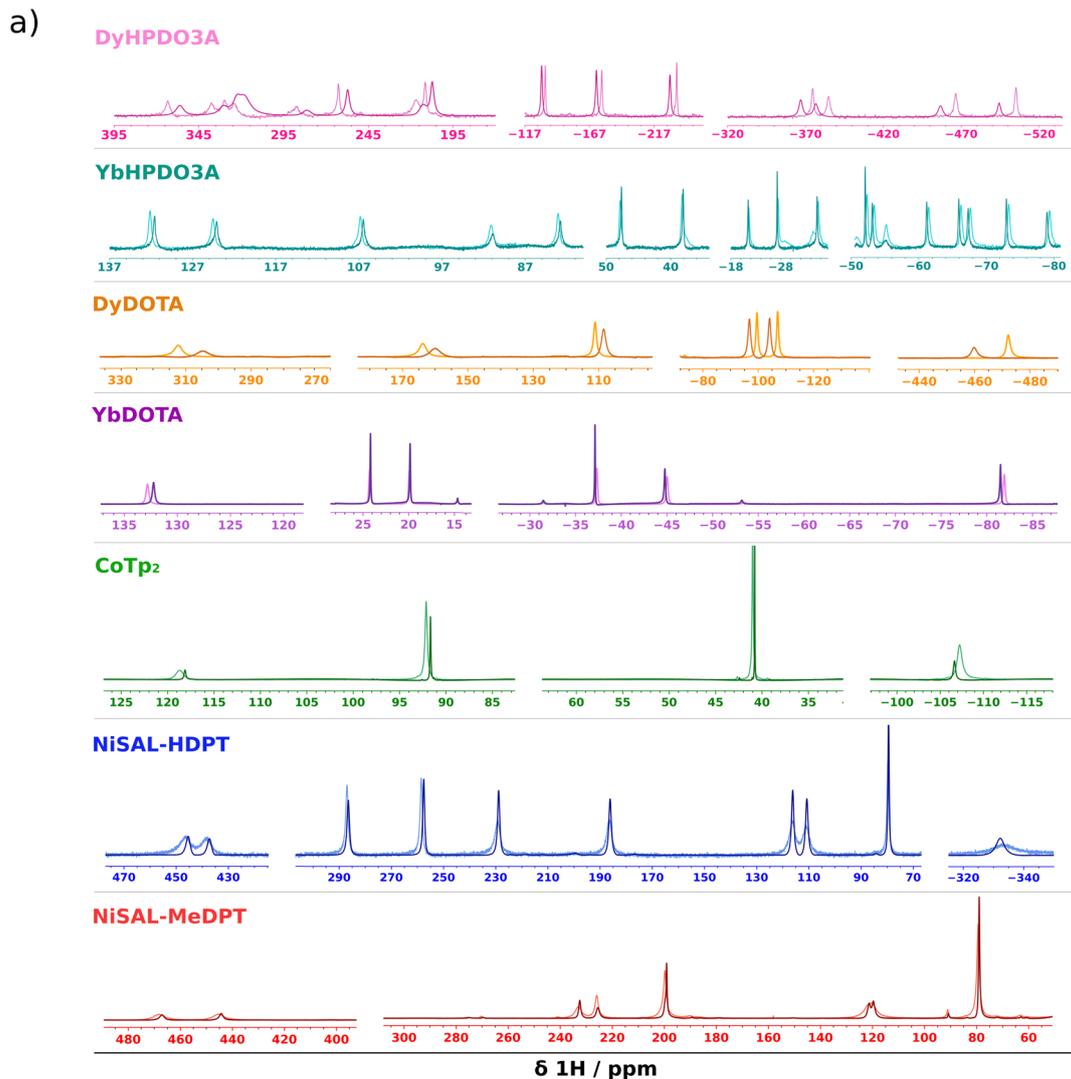
Fig. 1 (a) 1D ^{1}H NMR spectra of NiSAL-MeDPT, NiSAL-HDPT, CoTp$_2$, YbDOTA, DyDOTA, YbHPDO3A, and DyHPDO3A acquired at 400 MHz and 1.2 GHz. For each compound, the light-colored trace corresponds to the low field spectra, and the darker trace corresponds to the high field ones. (b) Correlation between the shifts collected at 1.2 GHz and 400 MHz at 298.0 K, showing a systematic reduction of the shift magnitude at higher fields, quantitatively supported by the slope of the least-squares regression line (given in parentheses).

Understanding the reduction of the shifts requires a detailed treatment recently proposed by some of us in ref. 16, through which the following expression is obtained for the field-dependent hyperfine shifts:

$$\delta \approx -\frac{1}{3}\boldsymbol{\sigma}^{(2:1)} + \left[\frac{1}{45}\frac{\beta}{\mu_0}\boldsymbol{\sigma}^{(2:1)}\boldsymbol{\chi}^{(2:1)} - \frac{1}{15}\frac{\beta}{\mu_0}(\boldsymbol{\sigma}\boldsymbol{\chi})^{(2:1)} - \frac{1}{5}\boldsymbol{\tau}^{(4:2)}\right]B_0^2 \tag{1}$$

where $\beta = 1/k_B T$, k_B is the Boltzmann constant, T is the absolute temperature, $\boldsymbol{\chi}$ is the magnetic susceptibility, and $\boldsymbol{\sigma}$ and $\boldsymbol{\tau}$ are the second- and fourth-order shielding tensors. The first and second order traces are reported as $\boldsymbol{\sigma}^{(2:1)} = \sum_i \sigma_{ii}$, and $\boldsymbol{\tau}^{(4:2)} = \sum_{ij}\tau_{iijj}$. We kept the same notation used by Ramsey.[6] Eqn (1) is obtained by third-order expansion of the field induced at the observed nuclei, with the quantities computed with zero applied magnetic field.[16]

These expressions are absolutely general, in that they are applicable also to closed-shell molecules. In ref. 16 and here, for simplicity, we neglected the orbital contribution† to the shielding, and focused on the hyperfine contribution. The latter is usually factorized, based on the nature of the interaction between the electron and the nucleus, into the Fermi contact (δ^{FC}) and the pseudocontact shift (δ^{PC}).[15] The first arises from nonzero spin density on the nuclei, while the latter is due to the through–space interaction of the nuclear spin with the induced average magnetic moment of the paramagnetic center.

The first term in eqn (1) is the field-independent contribution to the shift. The term proportional to B_0^2 encompasses the field-dependent effects. Within this latter term, the first two components represent the indirect effect,[14] whereas the third corresponds to the direct effect.[14] An intuitive way to understand this factorization is to consider that the indirect contribution arises from the partial alignment of molecules in solution due to the anisotropy of the magnetic susceptibility tensor,[17–22] whereas the direct contribution is given by a nonlinear response of the system to the magnetic field (comparable to the saturation of the total magnetic moment at high fields).

Both field-dependent contributions in eqn (1) can be reduced to familiar equations from paramagnetic NMR theory. If we restrict ourselves to the pseudocontact contribution to $\boldsymbol{\sigma}$ and to the point-dipole approximation (PDA), the two shielding tensors are given by[16]

$$\sigma_{lk} = -\frac{1}{4\pi R^3}\sum_q \chi_{lq}^{(1)}\left(\frac{3R^q R^k}{R^2} - \delta_{qk}\right), \tag{2}$$

$$\tau_{lmnk} = -\frac{1}{4\pi R^3}\sum_q \chi_{lmnq}^{(3)}\left(\frac{3R^q R^k}{R^2} - \delta_{qk}\right), \tag{3}$$

where $\chi^{(1)} \equiv \boldsymbol{\chi}$ is the usual second-order paramagnetic susceptibility tensor[23] and $\chi^{(3)}$ is an unusual fourth-order paramagnetic hypersusceptibility tensor. The two terms of the indirect contributions can easily be reduced to a $\boldsymbol{\chi}$-dependent self-orientation tensor (see section S1 for the proof).

In this work, we demonstrate the generality of the theory derived in ref. 16, and conduct a comprehensive analysis of the field effect across a broader range of paramagnetic systems, uncovering the non-trivial implications of the phenomenon.

2 Methods

2.1 NMR spectroscopy

The 1D ^{1}H NMR spectra were acquired for the following complexes: (i) NiSAL-HDPT[24] (SAL = salicylaldiminate; HDPT = N1-(3-aminopropyl)propane-1,3-diamine) dissolved in CDCl$_3$, (ii) NiSAL-MeDPT[24] (MeDPT = N1-(3-aminopropyl,3-methyl) propane-1,3-diamine) dissolved in CDCl$_3$, (iii) CoTp$_2$ (refs. 25 and 26) (Tp = tris(pyrazolyl)borate) dissolved in CDCl$_3$, (iv) YbDOTA[27,28] (DOTA = 1,4,7,10-tetraazacyclododecane-1,4,7,10-tetraacetic acid) dissolved in D$_2$O, (v) DyDOTA dissolved in D$_2$O, (vi) YbHPDO3A[29] (HPDO3A = 10-(2-hydroxypropyl)-1,4,7,10-tetraazacyclododecane-1,4,7-triacetic acid) dissolved in D$_2$O, and (vii) DyHPDO3A[29] dissolved in D$_2$O.

The experiments were recorded as a function of temperature and at two field values: 9.4 T and 28.2 T, corresponding to 400 MHz and 1.2 GHz ^{1}H Larmor frequency, respectively (see Table S1 for the acquisition parameters). The temperature was calibrated according to ref. 30 immediately before each acquisition session to ensure reproducibility between the two different instruments (see Section S2). For each sample, a series of spectra was acquired over a 2 K range centered around 298.0 K, in 0.2 K intervals. The temperature was equilibrated for 5 minutes before each acquisition. The chemical shift values were extracted from these series *via* an automated fitting procedure,[31] and the shift values at 298.00 K were then obtained through a linear regression, together with the corresponding uncertainties‡ (see Fig. S1–S18).

The assignment already available in ref. 29 for HPDO3A complexes is only partial. To compute the field dependence of the shifts and compare it to the experimental one, we completed and disambiguated the assignment as follows: starting from the *ab initio* computed tensor, we applied the combinatorial approach proposed earlier by Kuprov et al.,[32] which was then refined by an iterative, Monte-Carlo-like, tensor estimation–reassignment cycle. For YbHPDO3A, the assignment was further strengthened using the information from an EXSY spectrum. The full procedure is explained in section S3 (see also Fig. S19–S23 and Table S2 therein).

The EXSY spectrum, used in the assignment procedure, of YbHPDO3A was acquired at 400 MHz ^{1}H Larmor frequency using a $\pi/2 - d_0 - \pi/2 - d_8 - \pi/2 -$ acquisition sequence (noesyph of the Bruker standard library), where d_0 encodes for the time evolution in the indirect dimension. The mixing time d_8 was set to 5 ms.[29]

The full set of experimental shift values extracted from low- and high-field experiments, along with their corresponding assignments, is reported in Tables S3–S9 for all compounds.

2.2 Hyperfine shift simulation strategies

The simulated field-dependent hyperfine shifts were computed as a sum of the pseudocontact and the Fermi contact contributions as:

$$\delta = \delta^{PC} + \delta^{FC}, \tag{4}$$

with

$$\delta^{PC} = \delta^{PC,0} + \Delta\delta^{PC,\text{direct}} + \Delta\delta^{PC,\text{indirect}} \tag{5}$$

and

$$\delta^{FC} = \delta^{FC,0} + \Delta\delta^{FC,\text{direct}} + \Delta\delta^{FC,\text{indirect}}, \tag{6}$$

where δ^0 indicates the field-independent part of the shift, while $\Delta\delta^{\text{indirect}}$ and $\Delta\delta^{\text{direct}}$ represent the field-dependent indirect and direct contributions, respectively, and are collectively indicated as $\Delta\delta$. The complete set of equations is available in ref. 16.

According to the strategy used in this manuscript, the simulation of field-dependent hyperfine shifts requires the computation of the σ, χ and τ tensors, analytically, to be used in eqn (1), defined within a specific effective Hamiltonian. Possible options for this Hamiltonian are either to use ligand field/crystal field theory, or the Spin Hamiltonian (SH) parametrization. In the SH formalism, all the terms in the equation are expressed by means of the electron g-matrix g, the zero-field splitting tensor D, and hyperfine coupling tensors A. The δ^{FC} contributions are exclusively parameterized within this formalism, while the same is not necessarily true for δ^{PC}. For the latter, these equations can also be solved in the ligand-field approximation framework, defined by the Racah parameters for interelectronic interaction, the spin–orbit coupling constant, and the ligand field matrix elements.

In this work, all quantum chemical calculations were performed with ORCA software v6.0,[33] with the exception of the DFT calculations on NiSAL, performed with ORCA v5.0. For the hyperfine shift computation, we used the ParaMag.jl routines (available at: https://github.com/LucasLang/ParaMag.jl) according to the protocol available at https://github.com/LucasLang/fielddepshifts_analysis.

In general, δ^{FC} values were computed in the SH formalism from g, D, and A tensors, while δ^{PC} values were computed in the LF framework, using parameters from *ab initio* LF analysis (AILFT).[34,35] For transition metal complexes, the structures were optimized at the DFT level (see protocol (3) in S4) starting from the corresponding X-ray structures, when available, or from the closest analog (see section S4). AILFT parameters and D were computed at the CASSCF level with NEVPT2 correction (see protocol (1) in S4), and A and g at the DFT level (see protocol (4) in S4). For the cobalt(II) case, other combinations were also tested (*vide infra*). For the lanthanoid complexes, the structure optimization was performed with the same procedure as the transition metals, but for dysprosium analogues, the dysprosium(III) was substituted with yttrium(III), as suggested by Briganti *et al.* in ref. 36 for improved stability of the optimization. AILFT parameters were computed at the CASSCF level (see protocol (2) in S4).

3 Results and discussion

3.1 Theoretical considerations on limiting cases

Generally speaking, the two field-dependent contributions–the direct and the indirect–follow opposite trends: the field-induced

self-orientation increases the absolute value of the shift with increasing magnetic field, whereas the direct effect decreases it. Both $\Delta\delta^{\text{direct}}$ and $\Delta\delta^{\text{indirect}}$ exhibit the typical $d_{x^2-y^2}/d_{z^2}$ orbital-like shape in their isosurfaces. In fact, although one might expect the field-dependent shift contribution to PCSs by the τ tensor (see eqn (3)) to exhibit a higher-order angular dependence,[37] its application passes through a two-index contraction. Consequently, $\Delta\delta^{PC}$ retains a second-order spherical harmonics angular dependence as $\delta^{0,PC}$ (see Fig. S24). Based on geometrical arguments, the tensors that describe physical properties of a chemical system have to reflect its symmetry. For example, if the molecule has a symmetry axis of order higher than 2, the magnetic susceptibility tensor and the two-index contracted hypersusceptibility tensor will both be axial. As a result, $\Delta\delta^{\text{direct}}$ and $\Delta\delta^{\text{indirect}}$ will also have axial isosurfaces. If the starting tensors are rhombic, the $\Delta\delta^{\text{direct}}$ and $\Delta\delta^{\text{indirect}}$ contributions can have different rhombicity, and therefore the overall $\Delta\delta^{PC,\text{rel}}$ angular dependence will be more marked (*vide infra*).

The fact that the direct and the indirect effects follow opposite trends naturally raises the question: is it possible for the field-dependent contribution to be governed predominantly by either the direct or the indirect term, or will one always dominate? Insight into this question can be gained by considering limiting regimes.

In the SH framework, σ, χ, and τ can be expressed in powers of the inverse temperature. For transition metal complexes, if only the lowest non-vanishing terms are kept, we get the so-called high temperature (HT) limit, which translates into a $1/T$ dependence for σ and χ, and a $1/T^3$ dependence for τ. This limit is valid, as the name states, for high temperatures and/or vanishing zero-field splitting, conditions that are not quantitatively applicable for the model complexes presented in this work. However, in the HT limit of eqn (1), it is possible to derive qualitatively-reliable "rules of thumb" for the prediction of the ratios $\Delta\delta^{\text{rel}} = \Delta\delta/\delta^0$ for PCS and FCS, assuming the electronic g-factor $g_e = 2$ (see Section S5.1 for the derivation):

$$\Delta\delta^{PC,\text{rel}}_{HT} = \Delta\delta^{PC}/\delta^{PC,0} \approx -\beta^2\mu_B^2 B_0^2 \frac{8S^2 + 8S + 14}{75}, \tag{7}$$

$$\Delta\delta^{FC,\text{rel}}_{HT} = \Delta\delta^{FC}/\delta^{FC,0} \approx -\beta^2\mu_B^2 B_0^2 \frac{4S^2 + 4S + 2}{15}. \tag{8}$$

According to this prediction, the shift will always decrease with increasing field with an effect that depends only on temperature, B_0 and S. In fact, the equations in Section S5.1 show that $\Delta\delta^{FC}$ is exclusively determined by the direct effect, while $\Delta\delta^{PC}$ presents both contributions, with the direct always prevailing over the indirect, consequently leading to a global decrease of the shift with increasing field and a distinct field-dependent behavior of the two.

Along the same line, we can derive a general rule for the lanthanoid counterpart of the SH HT limit, in the range of validity of Bleaney's theory, where we can define an isotropic g value for each f^n ion, the so-called Landé g-factor g_J, that describes the proportionality of the total angular momentum $\mathbf{J}$ and the magnetic moment. In this case, the lowest-order terms in the $1/T$ expansion ($1/T$ for σ and $1/T^3$ for τ) vanish. Therefore,

we retain the next higher orders: $1/T^2$ for σ and $1/T^4$ for τ (details on this derivation are given in Section S5.2). Under these conditions, considering exclusively the PC contribution to the hyperfine shift,

$$\Delta\delta_{HT}^{rel} = \Delta\delta/\delta^0 \approx -\beta^2\mu_B^2 B_0^2 \frac{4J^2 + 4J + 5}{60}g_J^2. \tag{9}$$

This rule-of-thumb equation predicts that $\Delta\delta^{rel}$ depends only on the nature of the lanthanoid ion (J, g_J, as well as on B_0 and the temperature). To check the validity of this conclusion outside the approximations that we have taken to reach it, we verified–following eqn (1)–how large is the contribution from self-alignment when the anisotropy of the magnetic susceptibility is either very large or very small with respect to the magnetic susceptibility itself. We have hence selected two model crystal fields that produce limit-cases asphericities of the $4f^n$ electronic cloud for $n = 9$ (Dy^{3+}) and $n = 13$ (Yb^{3+}). For dysprosium(III), a strongly axial field (trigonal bipyramidal in this case) stabilizes the oblate density of the $M_J = 15/2$ state, yielding very large anisotropies,[38] whereas a strongly equatorial field (trigonal planar in the present case) stabilizes the $M_J = 1/2$ state, with a much smaller anisotropy. Ytterbium(III) has the opposite behavior (see Table 1). It is apparent that even with extreme anisotropies the direct contribution dominates. This demonstrates that the indirect and direct contributions are highly correlated, and it is not easy to modify one without modifying the other. Overall, the simulations performed on the model crystal fields are in very good qualitative agreement with the results of eqn (9).

3.2 Analysis of field dependence through some paramagnetic NMR archetypes

For all the signals that display a non-negligible paramagnetic contribution, the shift magnitudes decrease as the magnetic field increases (see Fig. 1 and Tables S3–S9). Because of the good resolution of the spectra, the effect is easily observable for all complexes. Even if the chemical shift ranges are similar (for e.g. NiSAL-HDPT and DyDOTA), the effect is stronger for the lanthanoid(III) complexes, reaching up to 12 ppm–more than 2.5% of the signal frequency–for the largest hyperfine shifts of DyDOTA. For transition metal complexes, the fraction of field-dependent hyperfine shift $\Delta\delta^{rel}$ is strongly dependent on the position of the proton, more so than in the case of lanthanoids.

This is related to the negligible contribution from δ^{FC} to the hyperfine shifts in lanthanoid complexes (vide infra).

When performing the simulations for comparison with the experimental data, we have to bear in mind a few limitations of the QC calculation of the observables:

1. DFT tends to overestimate electron delocalization.[40] For this reason, the hyperfine tensor at the observed nucleus is overestimated;

2. Multiconfigurational methods tend to underestimate covalency, hence overestimating the effect of spin orbit coupling. Consequently, g, D, and χ tend to be overestimated.

In line with previous work,[41] we use values from multiconfigurational methods for computing δ^{PC}, whereas for δ^{FC} we use a DFT-computed g-matrix, that is known to be underestimated and can potentially compensate for the overestimation of A values. In contrast, the D tensor is obtained from multiconfigurational methods.

A detailed description of the simulation strategy is provided in the Methods section and SI sections referenced therein.

For the nickel(II) complexes the Fermi contact term dominates, while for the cobalt(II) complex the pseudocontact term is predominant (see Fig. S27–S29). Our protocol consistently yields good agreement with the experimental data for the field-independent portion of the shifts, showing a very good correlation even in the cobalt(II) case, where we can observe some degree of overestimation (see Fig. 2 and Tables S12–S14).

When computing the field-dependent components of δ^{FC} and δ^{PC}, it becomes apparent that their trends with increasing magnetic field differ significantly (see Fig. S30–S32). This divergence originates from the fact that the field dependence of δ^{FC} arises almost entirely from the direct contribution $\Delta\delta^{direct}$, the indirect term being negligible. In contrast, for δ^{PC} both the direct and indirect components are significant: the direct contribution decreases the shift with increasing field, while the indirect contribution increases it. This is also perfectly in line with the rules of thumb of the previous section. Since the indirect effect is negligible for $\Delta\delta^{FC}$, the field effect on δ^{FC} is stronger than on δ^{PC}. It is important to stress that, even when the shifts are dominated by δ^{PC}, they decrease with the field because of the dominant $\Delta\delta^{direct}$.

Fig. 2 not only demonstrates satisfactory agreement between experimental and simulated $\Delta\delta$ values, but also clearly shows that the field-dependent contribution remains observable even with a potential low-to-high field temperature mismatch of 0.2

Table 1 Predicted fraction of field dependence of hyperfine shifts ($\Delta\delta^{rel} = \Delta\delta/\delta^0$) for Dy^{3+} and Yb^{3+} and two coordination geometries, trigonal planar (tp) and trigonal bipyramidal (tbp). The corresponding anisotropies, defined as $\Delta\chi_{ax} = \chi_{zz} - (\chi_{xx} + \chi_{yy})/2$, and magnetic susceptibility values, defined as $\chi_{iso} = (\chi_{xx} + \chi_{yy} + \chi_{zz})/3$, are also indicated, in m^3. The predicted $\Delta\delta^{rel}$ values are compared to the HT-approximated values from eqn (9) ($\Delta\delta_{HT}^{rel}$). The simulations were performed in the CF approximation with parameters computed using NJA-CFS software[39] as described in Section S5.2.1

|	tp			tbp			
f^n	$\Delta\delta^{rel}$(%)	$\Delta\chi_{ax} \times 10^{-31}$	$\chi_{iso} \times 10^{-31}$	$\Delta\delta^{rel}$(%)	$\Delta\chi_{ax} \times 10^{-31}$	$\chi_{iso} \times 10^{-31}$	$\Delta\delta_{HT}^{rel}$(%)
f^9 (Dy^{3+})	−2.52	−12.39	8.67	−2.37	24.23	9.13	−3.11
f^{13} (Yb^{3+})	−0.35	3.56	1.07	−0.33	−1.41	1.32	−0.60
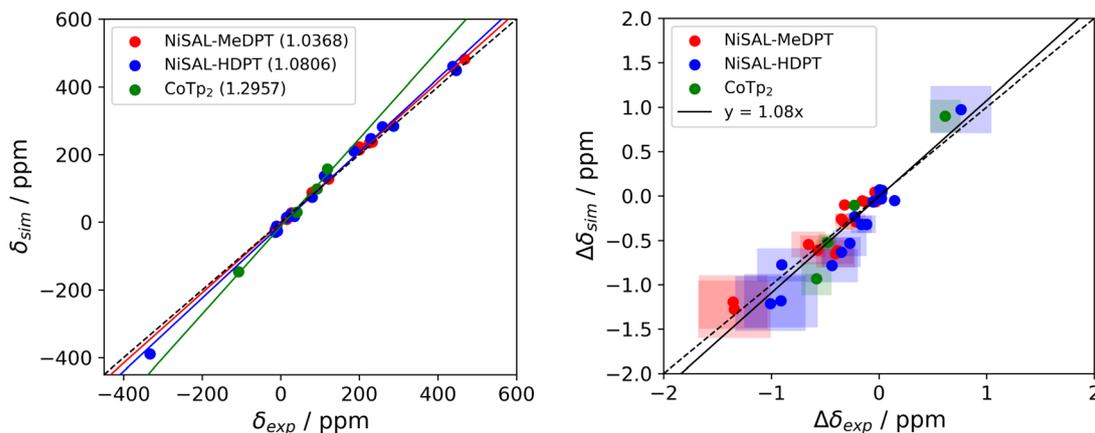
Fig. 2 Comparison of simulated field-dependent hyperfine shifts computed at 400 MHz ^{1}H Larmor frequency (left) and the correlation plot of the simulated ($\Delta\delta_{sim}$) field-dependent contribution to hyperfine shifts (right), defined as ($\delta_{1200\ MHz} - \delta_{400\ MHz}$), at 298.0 K, with the experimental counterpart, for transition metal complexes. The boxes represent the error introduced by a hypothetical 0.2 K mismatch between the spectra at different fields.

K (8 times the expected uncertainty and equivalent to the temperature calibration steps, see the Methods section).

A final remark can be made for the cobalt complex. In the literature, the preferred simulation strategy to reproduce the shifts in this system involves the computation of both δ^{PC} and δ^{FC} in the SH framework, using A from DFT calculations, while g and D are derived from an *ab initio* calculation (protocol B in Fig. S33 and Table S15).[42] When considering only the field-independent part, the results obtained with this combination of parameters are indeed superior to our results (protocol A in Fig. S33).§ However, when incorporating field-dependent effects, the first protocol predicts a trend three times stronger than what is observed experimentally, against the 1.5 times overestimation of our protocol, and $\Delta\delta^{rel}$ values that are very different from the experimental counterpart, that are, in contrast, very well reproduced by our protocol. We also tested the same purely SH-based approach while taking the HFC tensors from an *ab initio* calculation (protocol C in Fig. S33 and Table S16). This test revealed that, also in this case, the field-independent shifts are very well reproduced and the resulting field-dependence is very similar to protocol A; however, the agreement among $\Delta\delta^{rel}$ values is worse. We also took into account that this system cannot be fully described through the SH formalism,[25,43,44] and tested a different effective Hamiltonian involving the $^4T_{1g} \rightarrow {}^4P$ isomorphism (protocol D and E in Fig. S33).[44–46] If such an approach is taken, the results for the total shift are comparable to those of our protocol, and the $\Delta\delta$ values are also estimated quite well, even if, in this case, the $\Delta\delta^{rel}$ remains poorly predicted.¶

Considering all these simulations, we can therefore state that the best protocol from the field-dependence point of view (*i.e.*, based on both $\Delta\delta$ and $\Delta\delta^{rel}$) is the one proposed in this work, *i.e.* PCSs from AILFT and FCSs from SH with multi-configurational D and g, and A from DFT. From a methodological standpoint, this analysis implies that field dependence can serve as a calibration tool for the computational protocol, allowing one to obtain a more physically-meaningful Hamiltonian.

To study the effect beyond the transition metals, we have characterized the field dependence of two complexes of dysprosium(III) and ytterbium(III), DOTA and HPDO3A.

In the case of DOTA, the ratio of the magnetic anisotropy to the susceptibility is significantly larger for YbDOTA than for DyDOTA.[28,47,48] This can be rationalized as follows. The complex with bound water has C_1 symmetry, and the easy axis of DyDOTA is approximately perpendicular to the M–O$_W$ axis (where O$_W$ indicates the oxygen atom of the apical water molecule).[49] Given that the reorientation of water[50] and the molecular distortions (concerted rotation of the four acetic arms and conformational change of the macrocycle) are fast on the NMR timescale, the resulting susceptibility in solution is effectively axial, with its principal axis along the M–O$_W$ axis. For YbDOTA, since the electron density of the f orbitals is prolate, the principal axis is already along the M–O$_W$ axis even if no averaging is considered, due to the equatorial nature of the DOTA ligand.[51] Both complexes display two conformations: the square antiprismatic (SAP), which is dominant for the second half of the lanthanoid series, and the twisted square antiprismatic (TSAP), which has a lower molar fraction. The DOTA ligand itself occupies 8 coordination positions. In the TSAP conformer, water can be bound (in early lanthanoids) or not bound (in late lanthanoids). SAP and TSAP interconvert slowly on the NMR timescale, leading to distinct proton spectra. Fast equilibria with analogous structures lacking the capping water (SAP' and TSAP') also exist (see Fig. S34 and S35). For DyDOTA, the SAP and TSAP forms are the dominant slow-exchanging species, while for YbDOTA the slow exchange takes place between SAP and TSAP', with SAP being the most abundant for both complexes. Despite the fact that the complex with bound water is C_1-symmetric, the spectra only have six signals for each conformer (SAP and TSAP), which implies an effective C_4 symmetry for the ligand in solution, due to the fast rotation of the water around the M–O$_W$ axis. For this reason, in our simulations, the magnetic susceptibility anisotropy calculated *ab initio* was averaged over the 4 positions of minimum energy for

the water molecule identified by Briganti *et al.*,[36] as detailed in ref. 52. The averaging was performed by directly rotating the LF matrix elements from AILFT (see Section S6.2), and then, to obtain a single set of signals, the computed shift for each of the protons of DOTA was further averaged with its pseudosymmetry mates. However, it is important to stress that this "double average method" is only a pragmatic way to obtain a perfectly axial system (like the one we observe experimentally) and to approximate a far more complex equilibrium. For this reason, the corresponding simulated shift values are also reported as a simple single average over equivalent proton positions (see Tables S18 and S20).

As anticipated, the experimental shift values decrease with increasing magnetic field, an effect that is more pronounced in the dysprosium(III) complex than in the ytterbium(III) complex. If we look at $\Delta\delta^{\mathrm{rel}}$, we can notice that the field effect is very similar among different protons. This is in line with the axial character of the complex (as described in the previous section).

Given the largely ionic bonding in lanthanoid systems, in the simulation we neglected the δ^{FC} contribution. The δ^{PC} values were computed in the LF formalism. Additionally, the effective LF Hamiltonian was reduced to the same subspace of multiplicities used in the *ab initio* calculation from which the parameters were taken (see Section S6.2).

Our simulations successfully reproduced the experimental field dependence (see Fig. S38), showing a decrease in shift value with increasing field. This is attributed to the direct effect prevailing over the indirect contribution in $\Delta\delta^{\mathrm{PC}}$ (see Fig. S39 and S40), analogously to the transition metal case. For both complexes, however, we can clearly notice a large overestimation of the absolute value of the simulated hyperfine shift (see Fig. S38), which consequently leads to an overestimation of $\Delta\delta$ (see Fig. 3). This must be the reflection of the limitations introduced by the QC method itself, rather than a possible defect in the applied theory; in fact, the fraction of field-dependent contribution to the total shift $\Delta\delta^{\mathrm{rel}}$ is very close (on average) to the experimental counterpart: for dysprosium(III) SAP $\overline{\Delta\delta_{\mathrm{exp}}^{\mathrm{rel}}} = -2.483\%$ (*ab initio* $\Delta\delta^{\mathrm{rel}} = -2.732\%$) and ytterbium(III) SAP $\overline{\Delta\delta_{\mathrm{exp}}^{\mathrm{rel}}} = -0.438\%$ (*ab initio* $\Delta\delta^{\mathrm{rel}} = -0.489\%$) (see Tables S17–S20).

The experimentally observed position dependence of $\Delta\delta^{\mathrm{rel}}$, which is negligible in our simulations for both dysprosium(III) and ytterbium(III) complexes, likely derives from a minor yet distinct field-dependence of the contact shift, as seen in transition metal ions. Consequently, thanks to the negligible rhombicity of the magnetic susceptibility of this system, δ^{FC} could potentially be estimated in order to reproduce these differences, assuming a perfect $\Delta\delta^{\mathrm{PC}}$ simulation.
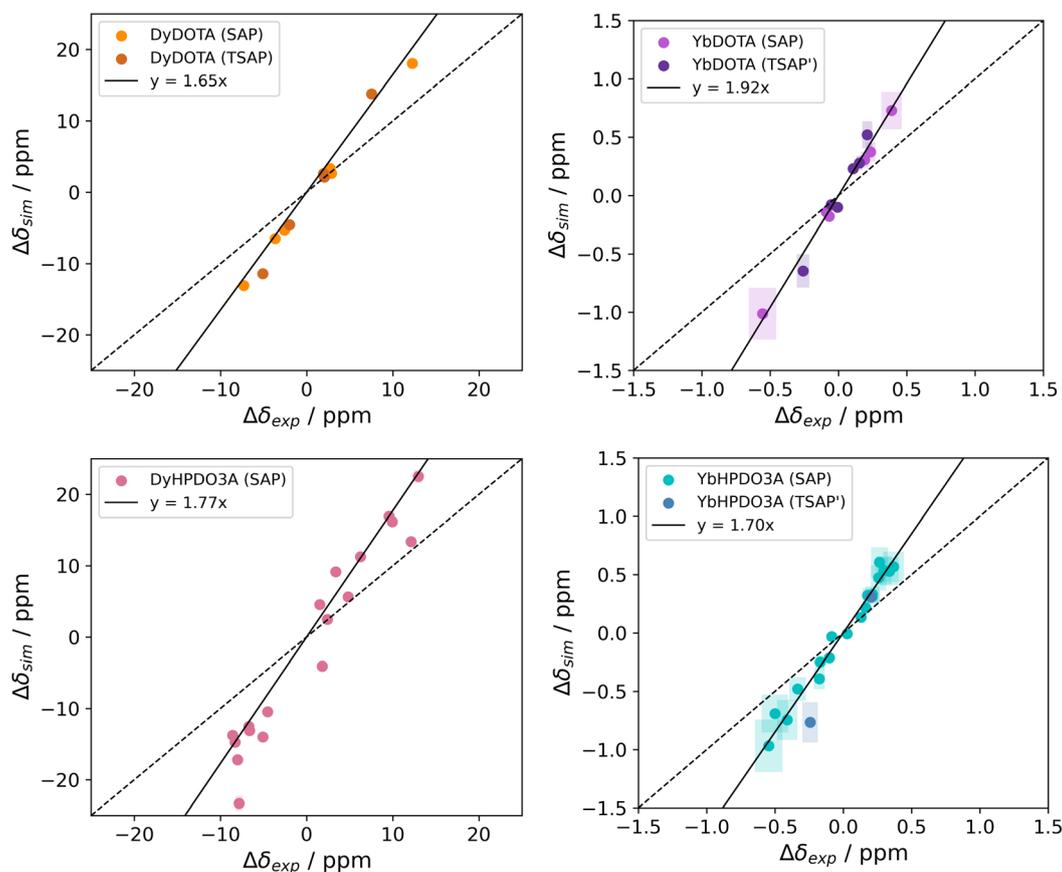
Fig. 3 Correlation plot of the simulated ($\Delta\delta_{\mathrm{sim}}$) and experimental ($\Delta\delta_{\mathrm{exp}}$) field-dependent contribution to hyperfine shifts, defined as ($\delta_{1200\ \mathrm{MHz}} - \delta_{400\ \mathrm{MHz}}$) at 298.0 K for DyDOTA and YbDOTA (above), and DyHPDO3A and YbHPDO3A (below). The boxes represent the error introduced by a hypothetical 0.2 K temperature mismatch between the spectra at different fields.

We can also notice that the ratio of $\Delta\delta^{\text{indirect}}/\Delta\delta^{\text{direct}}$ is higher for the ytterbium(III) analog. This is due to its greater susceptibility anisotropy with respect to the average susceptibility, compared to the dysprosium(III) analog.

The other set of lanthanoid(III) complexes, DyHPDO3A and YbHPDO3A, is a derivative of DOTA obtained by substituting one of the acetate groups with a hydropropyl group.[53] In this case, the C_4 pseudosymmetry is intrinsically broken. As a result, all the proton signals are visible in the spectra (see Fig. S22 and S23).[29] The susceptibility tensor obtained experimentally from the assignment procedure of DyHPDO3A and YbHPDO3A's signals in SAP conformations are very similar both in shape and direction to the *ab initio* ones, respectively $\Delta\chi_{\text{ax}} = -1.465 \times 10^{-30}$ m^3 (*ab initio*: -1.275×10^{-30} m^3) and $\Delta\chi_{\text{ax}} = -3.097 \times 10^{-31}$ m^3 (*ab initio*: -3.670×10^{-31} m^3); the complete tensors are reported in Table S2. The geometries are the same as those of DOTA, but additionally there is the configuration of the chiral center that has to be taken into account, leading to a total of eight isomeric forms potentially present in solution. Unlike DOTA, however, the enantiomers cannot interconvert in solution because they differ in the configuration of the chiral center, leaving two possible couples of SAP/TSAP conformers present in equilibrium. Also in this case, TSAP conformers are more common for lanthanoid ions at the beginning of the series, while SAP conformers are preferred for heavier ions. The exchange between TSAP and SAP (for dysprosium), or between SAP and TSAP' (for ytterbium), is slow on the NMR timescale, as two distinct sets of signals corresponding to these isomers can always be detected at 298 K. The structures used in this work for SAP and TSAP correspond to SAP1-S and TSAP1-R of ref. 29, proven to be the most abundant.

Fig. 4 Isosurfaces (at 50 ppm for δ^0 and 0.5 ppm for the field effects) for the YbDOTA (above) and YbHPDO3A (below) complexes, showing the field-independent and field-dependent PCS contributions, from left to right: δ^0, $\Delta\delta^{\text{direct}}$, $\Delta\delta^{\text{indirect}}$, and $\Delta\delta = \Delta\delta^{\text{direct}} + \Delta\delta^{\text{indirect}}$. These are computed as the difference between the shifts at zero field and those computed at a 1.2 GHz ^{1}H Larmor frequency, at 298 K. Simulation parameters are obtained from a CASSCF(13,7) calculation using ORCA (see protocol (2) in S4).

The experimental field dependence is very similar to the DOTA complexes, with the direct contribution higher than the indirect one, producing a decrease in the chemical shift with increasing magnetic field (see Fig. S38).

The simulation reproduced well the experimental field-dependence: for dysprosium(III) SAP $\overline{\Delta\delta^{\text{rel}}_{\text{exp}}} = -2.558\%$ (*ab initio* $\overline{\Delta\delta^{\text{rel}}} = -2.785\%$) and ytterbium(III) SAP $\overline{\Delta\delta^{\text{rel}}_{\text{exp}}} = -0.447\%$ (*ab initio* $\overline{\Delta\delta^{\text{rel}}} = -0.504\%$) (see Fig. 3 and Tables S21 and S22), despite the overestimation of the shifts in absolute values. This confirms that the field effect largely depends on the type of metal rather than on the particular symmetry and/or the ground state composition of the complex for systems with predominant axial character, in agreement with the Bleaney-like "rule of thumb" reported in the previous section. In this case we can notice that the variability of $\Delta\delta^{\text{rel}}$ produced by the different nuclear positions is higher compared to the DOTA analogs, due to the higher rhombicity induced by the low symmetry.

Regarding the composition of $\Delta\delta$, the same considerations made for DOTA are equally valid also in this case (see Fig. S41 and S42): $\Delta\delta^{\text{direct}}$ prevails and the ratio $\Delta\delta^{\text{PC,indirect}}/\Delta\delta^{\text{PC,direct}}$ is higher for the ytterbium(III) analog.

A plot of the isosurfaces of these two effects for YbDOTA and YbHPDO3A is shown in Fig. 4. As anticipated in the previous section, both $\Delta\delta^{\text{direct}}$ and $\Delta\delta^{\text{indirect}}$ exhibit the typical $d_{x^2-y^2}/d_{z^2}$ orbital-like shape in the PCS isosurfaces, with opposite signs for the two contributions. The final sign pattern is dictated by the $\Delta\delta^{\text{direct}}$ isosurfaces for both complexes, as the latter represents the largest contribution to the total $\Delta\delta$. Additionally, we can notice that the position dependence of $\Delta\delta^{\text{rel}}$ increases with the rhombicity of χ, showing that the "shape" of the field-effect reflects the symmetry of the system. The effect of the susceptibility is different for the indirect and direct components, and therefore their shapes can be different: indeed, the shapes of the two isosurfaces can differ in the case of non-axial symmetry, and even more significantly for lower symmetries.

4 Conclusions

The hyperfine interaction gives rise to observables that have been extensively used to study the structure of paramagnetic systems beyond the center of unpaired electron density.[15,54] Additionally, it has long been recognized that it can provide unique insights into both the electronic structure and the local geometry of the paramagnetic center itself.[22,55] Advancements in the understanding and interpretation of hyperfine-derived observables are therefore of broad significance, offering a deeper understanding of structure–function relationships in metal-based systems, and guiding the rational design of new functional materials and molecular architectures.

The present work offers a new perspective on this by demonstrating that the field-dependent component of the NMR hyperfine shift ($\Delta\delta$) constitutes an additional valuable observable that cannot be extracted from single-field data. The theoretical framework for its simulation, developed in a previous work by some of us,[16] is analyzed here in detail and employed to

delineate both the range of applicability and the potential of this newly defined observable.

The field-dependent contribution can be factorized into two terms: a direct term, which leads to a decrease in the shift as the magnetic field increases and originates from magnetic-moment saturation at high fields, and an indirect term, which produces the opposite effect, *i.e.* an increase in the shift with increasing field, due to field-induced self-orientation in solution. By approximating the previously-derived equations in the high-temperature limit, we find that the model predicts in all cases a decrease of the shift with increasing field, arising from the dominance of the direct term over the indirect one. This prediction is in full agreement with the experimental data for all investigated complexes, both transition-metal and lanthanoid. This implies that the saturation of the total magnetic moment plays a primary role in dictating how the shifts evolve with the magnetic field. Our results on DOTA and HPDO3A complexes further support this conclusion, as the fraction of the field-dependent contribution to the total shift is governed primarily by the nature of the lanthanoid ion itself, rather than by ligand-specific structural features.

Another observation from the present work is that, although typically small in magnitude, $\Delta\delta$ is highly sensitive to the balance between the Fermi contact (FC) and pseudocontact (PC) contributions. In transition-metal complexes, the markedly different field dependence of $\Delta\delta^{FC}$ (almost exclusively direct) and $\Delta\delta^{PC}$ (with substantial indirect contributions) makes the overall $\Delta\delta$ strongly dependent on the PC/FC ratio. Consequently, the experimental $\Delta\delta$ provides a stringent test of the relative weighting of these two contributions in computational or semi-empirical models: the agreement between measured and predicted field dependence validates the assumed FC/PC balance. For lanthanoid systems, where the FC term is conventionally considered negligible, the observed $\Delta\delta$ can provide qualitative information about the magnitude of this supposedly minor contribution, based on its dependence on the relative position of the observed nucleus with respect to the paramagnetic center, both in distance and orientation.

In this study, we demonstrated that the field-dependent component of NMR hyperfine shifts, albeit a secondary effect, may offer a promising avenue for improving the information available on the electronic structure of the paramagnetic center. Ultra-high-field NMR spectrometers are increasingly available, thus the systematic measurement of field-dependent hyperfine shifts offers new opportunities for NMR-based structural and electronic characterization.

Author contributions

Letizia Fiorucci: writing – conceptualization – original draft, software, methodology, investigation, formal analysis, data curation. Lucas Lang: writing – conceptualization, supervision – original draft, software, methodology – project administration, funding acquisition. David L. Tierney: writing – conceptualization – methodology. Mauro Botta: writing – conceptualization – methodology. Giacomo Parigi: writing – conceptualization – methodology. Claudio Luchinat: writing – conceptualization – methodology. Enrico Ravera: writing – conceptualization, supervision – original draft, methodology, investigation, data curation – project administration, funding acquisition.

Conflicts of interest

There are no conflicts to declare.

Data availability

The experimental data and the outputs of the calculations are available at https://zenodo.org/uploads/17981973.

Supplementary information (SI) is available. See DOI: https://doi.org/10.1039/d5sc09982j.

Acknowledgements

Notes and references

† In experimental literature, the total shift observed in closed-shell (diamagnetic) systems is often referred to simply as the diamagnetic shift, in contrast to paramagnetic shifts arising from unpaired electrons. Theoretically, however, this shift contains two distinct orbital contributions: the Lamb diamagnetic term, originating from the direct interaction of the magnetic field with the circulating bound electrons, and the Ramsey paramagnetic term, arising from field-induced mixing of excited electronic states (second-order paramagnetism).

‡ The temperature dependence of hyperfine shifts can be modeled in this case with a linear regression, given the narrow sampled temperature range.

§ The reassignment of the experimental ^1H NMR shifts of $CoTp_2$ proposed in ref. 42 is not correct and should be disregarded. This can be readily verified by inspection of the δ^0 PC isosurface in Fig. S24.

¶ Another option could be to include cubic Zeeman terms in the spin Hamiltonian for $CoTp_2$ (suggestion by Hélène Bolvin, private communication with Lucas Lang). In our case, this would affect only the FCSs and we neglect the effect in the following.

1 Z. Gan, *J. Magn. Reson.*, 2019, **306**, 86–90.

2 J.-H. Ardenkjaer-Larsen, G. S. Boebinger, A. Comment, S. Duckett, A. S. Edison, F. Engelke, C. Griesinger, R. G. Griffin, C. Hilty, H. Maeda, *et al.*, *Angew. Chem., Int. Ed.*, 2015, **54**, 9162–9185.

3 L. Banci, L. Barbieri, V. Calderone, F. Cantini, L. Cerofolini, S. Ciofi-Baffoni, I. C. Felli, M. Fragai, M. Lelli, C. Luchinat *et al.*, *arXiv*, 2019, preprint arXiv:1910.07462, DOI: 10.48550/arXiv.1910.07462.

4 H. Schwalbe, P. Audergon, N. Haley, C. A. Amaro, J. Agirre, M. Baldus, L. Banci, W. Baumeister, M. Blackledge, J. M. Carazo, *et al.*, *Structure*, 2024, **32**, 1563–1580.

5 R. W. Schurko, C. M. Rienstra, C. P. Jaroniec, A. L. Hansen, W. T. Franks, D. L. Bryce, A. Brinkmann, V. Terskikh, S. P. Brown, D. Iuga, *et al.*, *Solid State Nucl. Magn. Reson.*, 2025, 102053.

6 N. F. Ramsey, *Phys. Rev. A*, 1970, **1**, 1320.

7 M. R. Bendall and D. M. Doddrell, *J. Magn. Reson.*, 1979, **33**, 659–663.

8 D. Doddrell, D. Pegg and M. Bendell, *Aust. J. Chem.*, 1979, **32**, 1–10.

9 A. Boucekkine, G. Boucekkine-Yaker, M. N. Achour and G. Berthier, *J. Mol. Struct.:THEOCHEM*, 1988, **166**, 109–112.

10 K. Endo and K. Yamamoto, *J. Phys. Soc. Jpn.*, 1995, **64**, 4053–4054.

11 J. Vaara, P. Manninen and J. Lounila, *Chem. Phys. Lett.*, 2003, **372**, 750–757.

12 P. Manninen and J. Vaara, *Phys. Rev. A:At., Mol., Opt. Phys.*, 2004, **69**, 5.

13 J. Boyd, G. I. Pagola, M. C. Caputo, M. B. Ferraro and P. Lazzeretti, *J. Chem. Theory Comput.*, 2009, **5**, 1343–1349.

14 A. M. Kantola, P. Lantto, I. Heinmaa, J. Vaara and J. Jokisaari, *Phys. Chem. Chem. Phys.*, 2020, **22**, 8485–8490.

15 I. Bertini, C. Luchinat, G. Parigi and E. Ravera, *NMR of paramagnetic molecules: applications to metallobiomolecules and models*, Elsevier, 2016, vol. 2.

16 L. Lang, L. Fiorucci, G. Parigi, C. Luchinat and E. Ravera, *J. Chem. Theory Comput.*, 2025, **21**, 5642–5660.

17 J. Lohman and C. MacLean, *Chem. Phys.*, 1978, **35**, 269–274.

18 J. Lohman and C. MacLean, *Chem. Phys. Lett.*, 1978, **58**, 483–486.

19 A. Bothner-By, C. Gayathri, P. Van Zijl, C. MacLean, J.-J. Lai and K. M. Smith, *Magn. Reson. Chem.*, 1985, **23**, 935–938.

20 I. Bertini, I. C. Felli and C. Luchinat, High magnetic field consequences on the NMR hyperfine shifts in solution, 1998.

21 L. Heist, C.-D. Poon, E. Samulski, D. Photinos, J. Jokisaari, J. Vaara, J. W. Emsley, S. Mamone and M. Lelli, *J. Magn. Reson.*, 2015, **258**, 17–24.

22 G. Parigi, E. Ravera and C. Luchinat, *Prog. Nucl. Magn. Reson. Spectrosc.*, 2019, **114**, 211–236.

23 R. J. Kurland and B. R. McGarvey, *J. Magn. Reson.*, 1970, **2**, 286–301.

24 L. Sacconi and I. Bertini, *J. Am. Chem. Soc.*, 1966, **88**, 5180–5185.

25 W. K. Myers, E. N. Duesler and D. L. Tierney, *Inorg. Chem.*, 2008, **47**, 6701–6710.

26 T. N. Abell, R. M. McCarrick, S. L. Bretz and D. L. Tierney, *J. Chem. Educ.*, 2017, **94**, 1960–1964.

27 S. Aime, M. Botta and G. Ermondi, *Inorg. Chem.*, 1992, **31**, 4291–4299.

28 V. Jacques and J. F. Desreux, *Inorg. Chem.*, 1994, **33**, 4048–4053.

29 D. Delli Castelli, M. C. Caligara, M. Botta, E. Terreno and S. Aime, *Inorg. Chem.*, 2013, **52**, 7130–7138.

30 N. Karschin, S. Krenek, D. Heyer and C. Griesinger, *Magn. Reson. Chem.*, 2022, **60**, 203–209.

31 L. Fiorucci, F. Bruno, L. Querci, A. Kubrak, J. Bindi, N. Rodić, G. Licciardi, E. Luchinat, G. Parigi, M. Piccioli, *et al.*, *Magn. Reson. Chem.*, 2025, **63**, 628–654.

32 E. A. Suturina, K. Mason, C. F. Geraldes, I. Kuprov and D. Parker, *Angew. Chem.*, 2017, **129**, 12383–12386.

33 F. Neese, *Wiley Interdiscip. Rev.: Comput. Mol. Sci.*, 2025, **15**, e70019.

34 L. Lang, M. Atanasov and F. Neese, *J. Phys. Chem. A.*, 2020, **124**, 1025–1037.

35 M. Atanasov, S. V. Rao and F. Neese, *Chem. Sci.*, 2025, **16**, 18985–18989.

36 M. Briganti, G. F. Garcia, J. Jung, R. Sessoli, B. Le Guennic and F. Totti, *Chem. Sci.*, 2019, **10**, 7233–7245.

37 A. Buckingham and P. Stiles, *Mol. Phys.*, 1972, **24**, 99–108.

38 S. T. Liddle and J. van Slageren, *Chem. Soc. Rev.*, 2015, **44**, 6655–6669.

39 L. Fiorucci and E. Ravera, *J. Comput. Chem.*, 2025, **46**, e70063.

40 A. J. Cohen, P. Mori-Sánchez and W. Yang, *Chem. Rev.*, 2012, **112**, 289–320.

41 E. Ravera, L. Gigli, B. Czarniecki, L. Lang, R. Kuemmerle, G. Parigi, M. Piccioli, F. Neese and C. Luchinat, *Inorg. Chem.*, 2021, **60**, 2068–2075.

42 S. A. Rouf, J. Mares and J. Vaara, *J. Chem. Theor. Comput.*, 2015, **11**, 1683–1691.

43 B. R. McGarvey, *J. Chem. Phys.*, 1970, **53**, 86–91.

44 A. A. Pavlov, J. Nehrkorn, Y. A. Pankratova, M. Ozerov, E. A. Mikhalyova, A. V. Polezhaev, Y. V. Nelyubina and V. V. Novikov, *Phys. Chem. Chem. Phys.*, 2019, **21**, 8201–8204.

45 J. Jesson, *J. Chem. Phys.*, 1966, **45**, 1049–1056.

46 J. Jesson, S. Trofimenko and D. Eaton, *J. Am. Chem. Soc.*, 1967, **89**, 3148–3158.

47 L. Di Bari, G. Pescitelli, A. D. Sherry and M. Woods, *Inorg. Chem.*, 2005, **44**, 8391–8398.

48 E. M. Lopez-Vidal, M. Regueiro-Figueroa, M. D. García, C. Platas-Iglesias, C. Peinador and J. M. Quintela, *Inorg. Chem.*, 2012, **51**, 4429–4431.

49 G. Cucinotta, M. Perfetti, J. Luzon, M. Etienne, P. E. Car, A. Caneschi, G. Calvez, K. Bernot, R. Sessoli, *et al.*, *Angew. Chem., Int. Ed.*, 2012, **51**, 1606–1610.

50 P.-E. Car, M. Perfetti, M. Mannini, A. Favre, A. Caneschi and R. Sessoli, *Chem. Commun.*, 2011, **47**, 3751–3753.

51 M. Briganti, E. Lucaccini, L. Chelazzi, S. Ciattini, L. Sorace, R. Sessoli, F. Totti and M. Perfetti, *J. Am. Chem. Soc.*, 2021, **143**, 8108–8115.

52 F. S. Santana, M. Perfetti, M. Briganti, F. Sacco, G. Poneti, E. Ravera, J. F. Soares and R. Sessoli, *Chem. Sci.*, 2022, **13**, 5860–5871.

53 K. Kumar, C. A. Chang, L. Francesconi, D. Dischino, M. Malley, J. Gougoutas and M. Tweedle, *Inorg. Chem.*, 1994, **33**, 3567–3575.

54 E. Ravera, L. Gigli, L. Fiorucci, C. Luchinat and G. Parigi, *Phys. Chem. Chem. Phys.*, 2022, **24**, 17397–17416.

55 A. J. Pell, G. Pintacuda and C. P. Grey, *Prog. Nucl. Magn. Reson. Spectrosc.*, 2019, **111**, 1–271.